

# Hadron production by quark combination in central Pb+Pb collisions at $\sqrt{s_{NN}} = 17.3$ GeV

Chang-en Shao,<sup>1</sup> Jun Song,<sup>2</sup> Feng-lan Shao,<sup>1</sup> and Qu-bing Xie<sup>2</sup>

<sup>1</sup>*Department of Physics, Qufu Normal University, Shandong 273165, People's Republic of China*

<sup>2</sup>*Department of Physics, Shandong University, Shandong 250100, People's Republic of China*

The quark combination mechanism of QGP hadronization is applied to nucleus-nucleus collisions at top SPS energy. The yields, rapidity and transverse momentum distributions of identified hadrons in most central Pb+Pb collisions at  $\sqrt{s_{NN}} = 17.3$  GeV are systematically studied. The calculated results are in agreement with the experimental data from NA49 Collaboration. The longitudinal and transverse collective flows and strangeness of the hot and dense quark matter produced in nucleus-nucleus collisions at top SPS energy are investigated. It is found that the collective flow of strange quarks is stronger than light quarks, which is compatible with that at RHIC energies, and the strangeness is almost the same as those at  $\sqrt{s_{NN}} = 62.4, 130, 200$  GeV.

PACS numbers: 25.75.Dw, 25.75.Ld, 25.75.Nq, 25.75.-q

## I. INTRODUCTION

Lattice QCD predicts that at extremely high temperature and density, the confined hadronic matter will undergo a phase transition to a new state of matter called quark gluon plasma (QGP) [1, 2]. The relativistic heavy ion collisions can provide the condition to create this deconfined partonic matter [3]. In general, two approaches are used to study the properties of the deconfined hot and dense quark matter produced in AA collisions. One is studying the high  $p_T$  hadrons from initial hard jets, in which one can recur to the perturbative QCD to a certain degree [4]. The other is investigating the properties of thermal hadrons frozen out from the hot and dense quark matter. For the latter, the hadronization of the hot and dense quark matter (a typical non-perturbative process) is of great significance. Only through a reliable hadronization mechanism, can we reversely obtain various information of QGP properties from the final state hadrons measured experimentally. The abundant experimental data [5, 6] and phenomenological studies [7, 8, 9, 10, 11, 12] at RHIC energies suggest that quark combination mechanism is one of the most hopeful candidates. The two most noticeable results are the successful explanation of the high baryon/meson ratios and the constituent quark number scaling of the hadronic elliptic flow in the intermediate transverse momentum range [8, 9], which can not be understood at all in the partonic fragmentation picture. Recently, the NA49 Collaboration have measured the elliptic flow of identified hadrons at top SPS energy [13], and found that the quark number scaling of elliptic flow was shown to hold also. It immediately gives us an inspiration of the applicability for the quark combination at top SPS energy. On the other hand, the NA49 collaboration have found three interesting phenomena around 30A GeV [14], i.e. the steepening of the energy dependence for pion multiplicity, a maximum in the energy dependence of strangeness to pion ratio and a characteristic plateau of the effective temperature for kaon production. These phenomena are indicative of the onset of the deconfinement at low SPS energies. One can estimate via Bjorken method that the primordial spatial energy density in Pb+Pb collisions at top SPS energy is about

$3.0 \text{ GeV}/fm^3$  [15], exceeding the critical energy density (about  $1 \text{ GeV}/fm^3$ ) predicted by Lattice QCD. Therefore, the deconfined hot and dense quark matter has been probably created, and we can extend the quark combination mechanism to SPS energies.

As is well known, hadron yield is one of the most basic and important observables which can help us to test the understanding of the hadronization mechanism for the hot and dense quark matter created in the relativistic heavy ion collisions. In most of recombination/coalescence models, the hadron wave function is necessary to get the hadron yield. As the wave functions for almost all hadrons are unknown at present, it is difficult for these models to study this issue quantitatively [7, 8, 16]. In addition, these models do not satisfy the unitarity which is important to the issue as well [17]. Different from those models, the quark combination model [18, 19] uses the near-correlation in phase space and  $SU_f(3)$  symmetry, instead of hadron wave function, to determine the hadron multiplicity. In addition, the model satisfies unitarity as well and has reproduced many experimental data at RHIC [20, 21, 22, 23]. Therefore, we apply it in this paper to systematically study the yields, rapidity and transverse momentum distributions of various hadrons in most central Pb+Pb collisions at  $\sqrt{s_{NN}} = 17.3$  GeV. On one hand, one tests the applicability of the quark combination mechanism at this collision energy. We note that the first attempt of the mechanism at SPS energies, for hadron yields alone, was the ALCOR model [24, 25]. Now, the rich experimental data of hadron multiplicities and momentum spectra provide an opportunity to make a further, systematical and even decisive test of the mechanism at SPS energies. On the other hand, the parton momentum distributions at hadronization, which carry the information on the evolution of the hot and dense quark matter, are extracted from the final hadrons at top SPS energy and compared with those at RHIC energies. We concentrate the comparison on two properties related to strange hadron production. One is the difference in collective flow between light and strange quarks, which occurs at RHIC energies [23, 26]. The other is the strangeness enhancement, a significant property of QGP [27].

The paper is arranged as follows. In the next section, we make a brief introduction to the quark combination model. In section III, we calculate the yields and rapidity distributions of identified hadrons in most central Pb+Pb collisions at  $\sqrt{s_{NN}} = 17.3$  GeV. In section IV, the results of transverse momentum distributions of various hadrons are shown. In section V, we firstly make a detailed analysis of the longitudinal and transverse collective flow of the hot and dense quark matter at top SPS energy. Secondly, the energy dependence of the strangeness in the hot and dense quark matter is extracted and analyzed. Section VI presents summary.

## II. AN INTRODUCTION OF THE QUARK COMBINATION MODEL

The starting point of the model is a color singlet system which consists of constituent quarks and antiquarks. All kinds of hadronization models demand that they satisfy rapidity or momentum correlation for quarks in the neighborhood of phase space. The essence of this correlation is in agreement with the fundamental requirement of QCD [28]. According to QCD, a  $q\bar{q}$  may be in a color octet or a singlet. The color factors  $\langle (q\bar{q})_8 | \frac{\lambda^a \cdot \lambda^a}{4} | (q\bar{q})_8 \rangle = \frac{1}{6}$  and  $\langle (q\bar{q})_1 | \frac{\lambda^a \cdot \lambda^a}{4} | (q\bar{q})_1 \rangle = -\frac{4}{3}$ , which means a repulsive or an attractive interaction between them. Here  $\lambda^a$  are the Gell-Mann matrices. If they are close with each other in phase space, they can interact with sufficiently time to be in the color singlet and form a meson. Similarly, a  $qq$  can be in a sextet or an anti-triplet, and the color factors  $\langle (qq)_6 | \frac{\lambda^a \cdot \lambda^a}{4} | (qq)_6 \rangle = \frac{1}{3}$  and  $\langle (qq)_3 | \frac{\lambda^a \cdot \lambda^a}{4} | (qq)_3 \rangle = -\frac{2}{3}$ . If its nearest neighbor in phase space is a  $q$ , they form a baryon. If the neighbor is a  $\bar{q}$ , because the attraction strength of the singlet is two times that of the anti-triplet,  $q\bar{q}$  will win the competition to form a meson and leave a  $q$  alone to combine with other quarks or antiquarks. Based on the above QCD and near-correlation in phase space requirements, we had proposed a quark combination rule(QCR) [18, 28] which combines all these quarks and antiquarks into initial hadrons. When the transverse momentum of quarks are negligible, all  $q$  and  $\bar{q}$  can always line up stochastically in rapidity. The QCR reads as follows:

1. Starting from the first parton ( $q$  or  $\bar{q}$ ) in the line;
2. If the baryon number of the second in the line is of the different type from the first, i.e. the first two partons are either  $q\bar{q}$  or  $\bar{q}q$ , they combine into a meson and are removed from the line, go to point 1; Otherwise they are either  $qq$  or  $\bar{q}\bar{q}$ , go to the next point;
3. Look at the third, if it is of the different type from the first, the first and third partons form a meson and are removed from the line, go to point 1; Otherwise the first three partons combine into a baryon or an anti-baryon and are removed from the line, go to point 1.

The following example shows how the above QCR works

$$\begin{aligned} & q_1 \bar{q}_2 \bar{q}_3 \bar{q}_4 \bar{q}_5 q_6 \bar{q}_7 q_8 q_9 q_{10} \bar{q}_{11} q_{12} q_{13} q_{14} \bar{q}_{15} q_{16} q_{17} \bar{q}_{18} \bar{q}_{19} \bar{q}_{20} \\ & \rightarrow M(q_1 \bar{q}_2) \bar{B}(\bar{q}_3 \bar{q}_4 \bar{q}_5) M(q_6 \bar{q}_7) B(q_8 q_9 q_{10}) M(\bar{q}_{11} q_{12}) \\ & M(q_{13} \bar{q}_{15}) B(q_{14} q_{16} q_{17}) \bar{B}(\bar{q}_{18} \bar{q}_{19} \bar{q}_{20}) \end{aligned}$$

If the quarks and antiquarks are stochastically arranged in rapidity, the probability distribution for  $N$  pairs of quarks and antiquarks to combine into  $M$  mesons,  $B$  baryons and  $B$  anti-baryons is

$$X_{MB}(N) = \frac{2N(N!)^2(M+2B-1)!}{(2N)!M!(B!)^2} 3^{M-1} \delta_{N,M+3B}. \quad (1)$$

Hadronization is the soft process of the strong interaction and is independent of flavor, so the net flavor number remains constant during the process. In the quark combination scheme, this means that the quark number for each certain flavor prior to hadronization equals to that of all initially produced hadrons after it. Obviously the quark number conservation is automatically satisfied in the model. It is different from the non-linear algebraic method in ALCOR model [24] where normalization factor for each quark flavor is introduced with the constraint of the quark number conservation.

The average number of initially produced mesons  $M(N)$  and baryons  $B(N)$  are given by

$$\langle M(N) \rangle = \sum_M \sum_B M X_{MB}(N), \quad (2)$$

$$\langle B(N) \rangle = \sum_M \sum_B B X_{MB}(N). \quad (3)$$

Then the multiplicity of various initial hadrons is obtained according to their production weights

$$\langle M_j^{initial} \rangle = C_{M_j} \langle M(N) \rangle, \quad \langle B_j^{initial} \rangle = C_{B_j} \langle B(N) \rangle, \quad (4)$$

where  $C_{M_j}$  and  $C_{B_j}$  are normalized production weights for the meson  $M_j$  and baryon  $B_j$ , respectively. If three quark flavors are considered only, we can obtain the production weights using the  $SU_f(3)$  symmetry with a strangeness suppression factor  $\lambda_s$  [18, 19], which are listed in Table I. The extension of the symmetry to excited states, exotic states and more quark flavors is also straightforward [19, 22, 29].

Considering the decay contributions from the resonances, we can obtain the yields of final state hadrons

$$\langle h_i^{final} \rangle = \langle h_i^{initial} \rangle + \sum_j B_r(j \rightarrow i) \langle h_j \rangle, \quad (5)$$

where the  $B_r(j \rightarrow i)$  is the weighted decay branching ratio for  $h_j$  to  $h_i$  [30].

In principle, the hadron production probability should be calculated from the matrix element  $\langle q\bar{q} | M \rangle$  for meson or  $\langle qq\bar{q} | B \rangle$  for baryon. However, the wave functions for almost all hadrons which are governed by the non-perturbative QCD are unknown at present. It is difficult

TABLE I: The normalized production weight for baryons and mesons in the  $SU_f(3)$  ground state.  $r_i$  is the number of strange quarks in hadron. The ratio of the vector ( $J^P = 1^-$ ) to pseudoscalar ( $J^P = 0^-$ ) meson follows the spin counting, while that of the decouplet ( $J^P = \frac{3}{2}^+$ ) to octet ( $J^P = \frac{1}{2}^+$ ) baryon suffers a spin suppression effect; see Ref. [19, 29] for details.

$C_M$	$C_{M_i} = \frac{2J_i+1}{4(2+\lambda_s)^2} \lambda_s^{r_i}$ , except	
	$C_\eta = \frac{2J_\eta+1}{4(2+\lambda_s)^2} \frac{1+2\lambda_s^2}{3}$	$C_{\eta'} = \frac{2J_{\eta'}+1}{4(2+\lambda_s)^2} \frac{2+\lambda_s^2}{3}$
$C_B$	$C_{B_i} = \frac{4}{(2+\lambda_s)^3(2J_i+1)} \lambda_s^{r_i}$ , except	
	$C_\Lambda = C_{\Sigma^0} = C_{\Sigma^+0} = C_{\Lambda(1520)} = \frac{3}{2(2+\lambda_s)^3} \lambda_s$	

to study the production of hadrons quantitatively through their wave functions. In view of this, the hadron production probability in our model is determined by the  $SU_f(3)$  symmetry with a strangeness suppression. This symmetry has been supported by many experiments, particularly by the coincidence of the observed  $\lambda_s$  obtained from various mesons and baryons [31]. Therefore, the model can quantitatively describe many global properties for the bulk system by virtue of the Monte Carlo method [19, 20, 21, 22, 23, 29].

When applying the model to describe the hadronization of the hot and dense quark matter produced in heavy ion collisions, the net-baryon quantum number of the system perplexes the analysis formula of Eq. 1 but it can be easily evaluated in Monte Carlo program. On the other hand, the transverse momentum of quarks is not negligible due to the strong collective flow of quark matter. In principle, we should define the QCR in three-dimensional phase space, but it is quite complicated to have it because one does not have an order or one has to define an order in a sophisticated way so that all quarks can combine into hadrons in a particular sequence. In practice, the combination is still put in rapidity and meanwhile the maximum transverse momentum difference  $\Delta_p$  between (anti)quarks are constrained as they combine into hadrons. The transverse spectra of hadrons have a relationship with the quark spectra as follows (e.g. for meson)

$$\frac{dN_M}{d^2\mathbf{p}_T} \propto \int d^2\mathbf{p}_{1,T} d^2\mathbf{p}_{2,T} f_q(\mathbf{p}_{1,T}) f_{\bar{q}}(\mathbf{p}_{2,T}) \delta^2(\mathbf{p}_T - \mathbf{p}_{1,T} - \mathbf{p}_{2,T}) \times \Theta(\Delta_p - |\mathbf{p}_{1,T}^* - \mathbf{p}_{2,T}^*|), \quad (6)$$

where  $f_{q/\bar{q}}(\mathbf{p}_T)$  is the transverse momentum distribution of the quark/antiquark, assumed to be rapidity-independent in present work. The superscript asterisk denotes the quark momentum in the center-of-mass frame of formed hadron. The limitation  $\Delta_p$  is treated as parameter in our study, and fixed to be  $\Delta_p = 0.3$  GeV for mesons and  $\Delta_p = 0.6$  GeV for baryons both at RHIC and SPS energies. Note that the spectrum normalization is determined by the multiplicity in Eq. 4, i.e. the constraint of the parameter  $\Delta_p$  on the hadron yield is neglected.

One issue that is often questioned is the energy and entropy conservation in quark combination process. As the non-perturbative QCD is unsolved, there is no rigorous

theory which can incorporate the partonic phase as well as hadronic phase, thus it is difficult to justify or condemn this issue in essence at the moment. As we know, a lot of the experimental phenomena in intermediate transverse momentum range at RHIC can be explained beautifully only in the quark combination scenario. It suggests that maybe this 'puzzling' issue does not exist. As far as the quark combination itself is concerned, there is no difference for the combination occurred in the different (intermediate or low) transverse momentum range. Therefore, whether the properties of low  $p_T$  hadrons can be reproduced or not is also a significant test of the quark combination mechanism, as the vast majority of hadrons observed experimentally are just these with low transverse momentum.

### III. HADRON YIELDS AND RAPIDITY DISTRIBUTIONS

In high energy nucleus-nucleus collisions, the energy deposited in the collision region excites large numbers of newborn quarks and antiquarks from the vacuum. Subsequently, the hot and dense quark matter mainly composed of these newborn quarks will expand hydrodynamically until hadronization. The net-quarks from the colliding nuclei still carry a fraction of beam energy, thus their evolution is different from the newborn quarks. One part of net-quarks are stopped in the hot and dense quark matter, and hadronize together with it. The other part of net-quarks penetrate the hot quark matter, and run up to the forward rapidity region. The latter, together with small amount newborn quarks, form the leading fireball. Their hadronization should be earlier than that of the hot and dense quark matter with a prolonged expansion stage, and the hadronization outcomes consist of nucleons and small amount of mesons.

The current version of quark combination model simulates only the hadronization of the hot and dense quark matter and subsequently decays of resonances. One in-

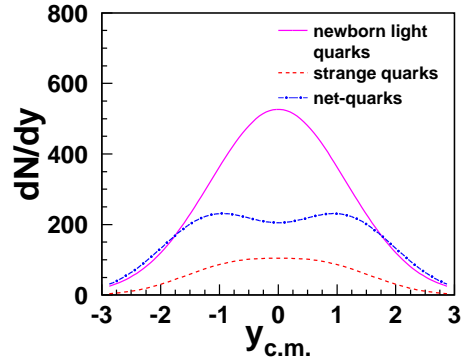


FIG. 1: (Color online) Rapidity spectra of newborn quarks and net-quarks at hadronization in most central Pb+Pb collisions at  $\sqrt{s_{NN}} = 17.3$  GeV.

dispensable input is the momentum distributions of thermal quarks and antiquarks at hadronization, which are the results of the hydrodynamic evolution in partonic phase. In order to focus attentions on the test of quark combination mechanism in this and next sections, we reversely extract the quark distributions by fitting the experimental data in the model. A detailed analysis of quark distributions at hadronization will be in section V. The solid and dashed lines in Fig. 1 show the rapidity distributions of newborn light and strange quarks at hadronization respectively, obtained from the  $\pi^-$  and  $K^+$  data [32]. The dotted-dashed line is the rapidity distribution of net-quarks in the hot and dense quark matter, which is extracted from net-proton data [33].

Firstly, we calculate the yields and rapidity densities at midrapidity of various hadrons in most central Pb+Pb collisions at  $\sqrt{s_{NN}} = 17.3$  GeV. The results are shown in Table II. From the energy dependence of the rapidity density for net-baryon [39], one can see that the nucleus-nucleus collisions at SPS energies exhibit a strong stopping power. Therefore, the leading particles contribute little to yields and rapidity distributions of various hadrons.

The calculated yields and rapidity densities of vector meson  $\phi$  are shown to be about twice as high as the experimental data. The results of other hadrons are basically in agreement with the experimental data, but slight deviations exist also. The overpredictions of  $\phi$  meson may be associated with the exotic particle  $f_0(980)$ , which has a possible tetraquark structure containing a strange quark and a strange antiquark [40]. As a bond state containing strange components, it has a slightly lower mass than  $\phi$  meson but is not included in the  $SU_f(3)$  ground states. In the present work, we consider only the production of 36 – *plets* of meson and 56 – *plets* of baryon in the  $SU_f(3)$  ground states, and the excited states and exotic states are not taken into account. The  $f_0(980)$  multiplicity is found to be nearly the same as  $\phi$  meson in the  $e^+e^-$  annihilations [30]. The  $m_T$  distribution of  $f_0(980)$  measured by STAR Collaboration in Au+Au collisions at  $\sqrt{s_{NN}} = 200$  GeV is also shown to be comparable to that of  $\phi$  [41, 42]. Therefore, the overprediction of  $\phi$  meson can be removed by incorporating the  $f_0(980)$  production.

Subsequently, we will calculate the longitudinal rapidity distributions of various hadrons. Due to the deviations in hadron yields, it is difficult to directly compare the calculated hadron spectra with the experimental data. In order to focus attentions on the property of hadron momentum spectra, we will scale the calculated rapidity densities to the center value of the experimental data when we show the hadronic rapidity and  $p_T$  spectra in Fig. 2 and 4 respectively, thereby removing these deviations in hadron yields.

Pion is the lightest and most abundant hadron produced in AA collisions, and its momentum distribution can best reflect the global evolution property of the hot and dense quark matter. In various models of high energy heavy ion collisions, the reproduction of pion meson is always taken as a paramount test of models. In Landau hydrodynamic model [43], the rapidity distribution of pion can be well

TABLE II: The yields (left) and rapidity densities at midrapidity (right) of identified hadrons in central Pb+Pb collisions at  $\sqrt{s_{NN}} = 17.3$  GeV. The experimental data are taken from Ref. [32, 34, 35, 36, 37, 38]

	yield		$\frac{dN}{dy} _{y=0}$	
	data	model	data	model
$\pi^+$	$619 \pm 17 \pm 31$	566	$170.1 \pm 0.7 \pm 9$	168.2
$\pi^-$	$639 \pm 17 \pm 31$	630	$175.4 \pm 0.7 \pm 9$	183.5
$K^+$	$103 \pm 5 \pm 5$	92.5	$29.5 \pm 0.3 \pm 1.5$	27.3
$K^-$	$51.9 \pm 1.6 \pm 3$	45.3	$16.8 \pm 0.2 \pm 0.8$	15.7
$K_s^0$	$75 \pm 4$	66.7	$26.0 \pm 1.7 \pm 2.6$	20.7
$\phi$	$8.46 \pm 0.38 \pm 0.33$	15.2	$2.44 \pm 0.1 \pm 0.08$	5.26
$p$		120	$29.6 \pm 0.9 \pm 2.96$	25.9
$\bar{p}$		3.2	$1.66 \pm 0.17 \pm 0.17$	1.53
$\Lambda$	$44.9 \pm 0.6 \pm 8$	52.9	$9.5 \pm 0.1 \pm 1.0$	13.3
$\bar{\Lambda}$	$3.07 \pm 0.06 \pm 0.31$	2.88	$1.24 \pm 0.03 \pm 0.13$	1.35
$\Xi^-$	$4.04 \pm 0.16 \pm 0.57$	4.9	$1.44 \pm 0.1 \pm 0.15$	1.43
$\Xi^+$	$0.66 \pm 0.04 \pm 0.08$	0.58	$0.31 \pm 0.03 \pm 0.03$	0.26

described and the sound velocity (which is an important physical quantity standing for the property of the hot and dense quark matter) can be extracted from the pion distribution. For other hadrons, such as kaons, protons,  $\Lambda$ ,  $\Xi$  and so on, the Landau model can not describe their rapidity distributions with the same sound velocity or freeze-out temperature [44, 45, 46]. For a systematic description of the rapidity distributions of various hadrons, the detailed longitudinal dynamics, e.g. the evolution of net-baryon density which will result in the yield and spectrum asymmetry between hadron and antihadron, should be included. In addition, the hadronization mechanism is especially important to describe the differences in the yield and momentum distribution of various hadron species. Using the extracted quark distributions in Fig. 1, we calculate the rapidity distributions of pions, kaons,  $\Lambda(\bar{\Lambda})$ ,  $\Xi^-(\bar{\Xi}^+)$  and  $\phi$  in most central Pb+Pb collisions at  $\sqrt{s_{NN}} = 17.3$  GeV. The results are shown in Fig. 2 and are compared with the experimental data. The calculated rapidity spectrum of  $\phi$  meson is narrow than the latest data of NA49 Collaboration (open circles in the second panel), but is in good agreement with previous data (filled circles). The rapidity spectra of other hadrons are well reproduced. One can see that the quark combination mechanism is applicable for describing the longitudinal distributions of various hadrons at top SPS energy.

#### IV. HADRON TRANSVERSE MOMENTUM DISTRIBUTIONS

In this section, we calculate the transverse momentum distributions of various hadrons in the midrapidity range. In this paper, we only consider the hadronization of the hot and dense quark matter. The transverse momentum invariant distribution of constituent quarks at hadronization is



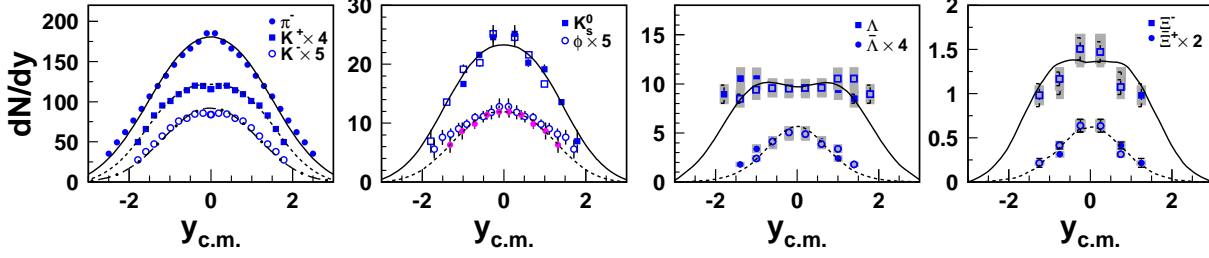


FIG. 2: (Color online) The scaled rapidity distributions of identified hadrons in most central Pb+Pb collisions at  $\sqrt{s_{NN}} = 17.3$  GeV. The contributions from leading particles are not included. The open circles of  $\phi$  data in the second panel are the latest results measured by NA49 Collaboration [35], and filled circles are the previous ones [47]. Other experimental data are taken from Ref. [32, 37, 38]. The open symbols of  $K_s^0$ ,  $\Lambda$  and  $\Xi$  show data points reflected around midrapidity.

taken to be an exponential form  $\exp(-m_T/T)$ , where  $T$  is the slope parameter which is also called effective production temperature. Fig. 3 shows the midrapidity  $p_T$  spectra of constituent quarks at hadronization in most central Pb+Pb collisions at  $\sqrt{s_{NN}} = 17.3$  GeV. The spectra of newborn light and strange quarks are extracted from the data of  $\pi^+$  and  $K^+$  respectively [48]. The net-quark distribution is fixed by the data of  $K^-/K^+$  ratio as a function of  $p_T$  [48]. A detailed analysis of the quark  $p_T$  spectra will be shown in section V.

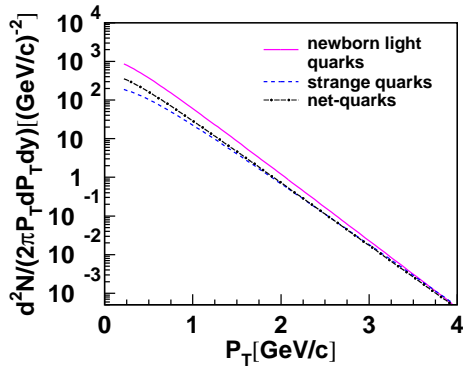


FIG. 3: (Color online) The transverse momentum distributions of constituent quarks in the midrapidity region at hadronization in most central Pb+Pb collisions at  $\sqrt{s_{NN}} = 17.3$  GeV.

Fig. 4 shows the calculated  $p_T$  spectra of pions, kaons, protons,  $\Lambda(\bar{\Lambda})$ ,  $\Xi^-(\bar{\Xi}^+)$  and  $\phi$  in most central Pb+Pb collisions at  $\sqrt{s_{NN}} = 17.3$  GeV. For kaons, protons,  $\Lambda$  and  $\Omega$ , the spectral slopes of antihadrons measured experimentally are all steeper than those of hadrons [48, 49, 50]. However, the spectrum of  $\Xi^-$  is abnormally steeper than that of  $\bar{\Xi}^+$  [37]. Our predictions are in good agreement with all the data except  $\Xi^-$ .

The exponential function  $\exp(-m_T/T)$  is often used experimentally to fit the transverse momentum distributions of identified hadrons in the low  $p_T$  range, and to extract

the effective production temperature  $T$  of various hadrons. It is found at top SPS energy that all final-state hadrons except pion meson have much higher  $T$  than the critical temperature [51], which indicates a strong collective flow at this collision energy. It is regarded in Ref. [52] that this observed flow mainly develops in the late hadronic rescattering stage. But results in Fig. 2 and Fig. 4 all show that both longitudinal and transverse spectra of various hadrons can be coherently explained by the same quark distributions, respectively. It suggests that the observed flow should mainly come from the expansive evolution stage of the hot and dense quark matter before hadronization, but not from the post-hadronization stage. In addition, the same constituent quark spectra contained in light, single- and multi- strange hadrons also imply that the hot quark matter hadronize into these initial hadrons almost at the same time, i.e. the hadronization is a rapid process.

In Fig. 5, we calculate the  $p_T$  spectra of pions, kaons, protons,  $\Lambda(\bar{\Lambda})$ ,  $\Xi^-(\bar{\Xi}^+)$ ,  $\phi$  and  $\Omega(\bar{\Omega})$  in most central Au+Au collisions at top RHIC energy. The momentum distributions of constituent quarks at hadronization are taken to be  $\exp(-m_T/0.375)$  for strange quarks and  $\exp(-m_T/0.34)$  for light quarks. The numbers and rapidity spectra of the light and strange quarks and antiquarks have been obtained in the study of the longitudinal hadron production [55]. Here, the result of  $\phi$  meson is multiplied by a factor 0.5. One can see that the  $p_T$  spectra of various hadrons are well reproduced.

The baryon/meson ratio as a function of  $p_T$  is sensitive to the hadronization mechanism. As we know, the observed high baryon/meson ratios in the intermediate  $p_T$  range at RHIC energies [5] can not be understood at all in the scheme of parton fragmentation, but can be easily explained in the quark combination mechanism. Fig. 6 shows the model predictions of  $\bar{p}/\pi^-$ ,  $\Lambda/K_s^0$  and  $\Omega/\phi$  at midrapidity in both central Pb+Pb collisions at  $\sqrt{s_{NN}} = 17.3$  GeV and central Au+Au collisions at  $\sqrt{s_{NN}} = 200$  GeV. In the intermediate  $p_T$  range where the hadron production is dominated by the combination of thermal quarks, the baryon/meson ratios increase with the

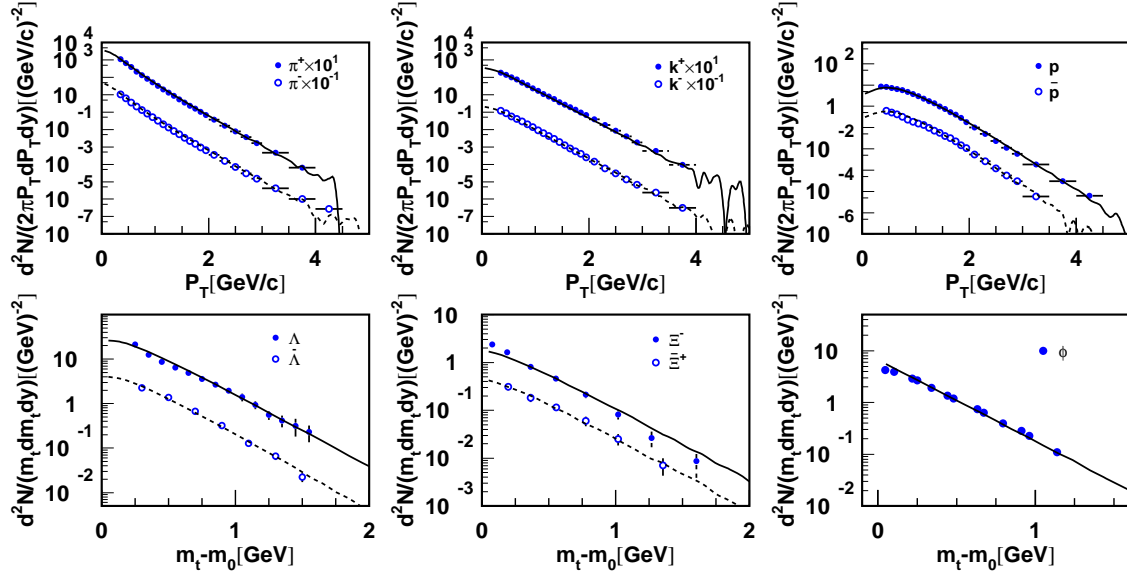


FIG. 4: (Color online) The scaled transverse momentum distributions of identified hadrons at midrapidity in most central Pb+Pb collisions at  $\sqrt{s_{NN}} = 17.3$  GeV. Only the combination of thermal quarks is taken into account. Solid lines are the calculated results of hadrons and dashed lines for antihadrons. The experimental data are from Ref. [35, 37, 48]

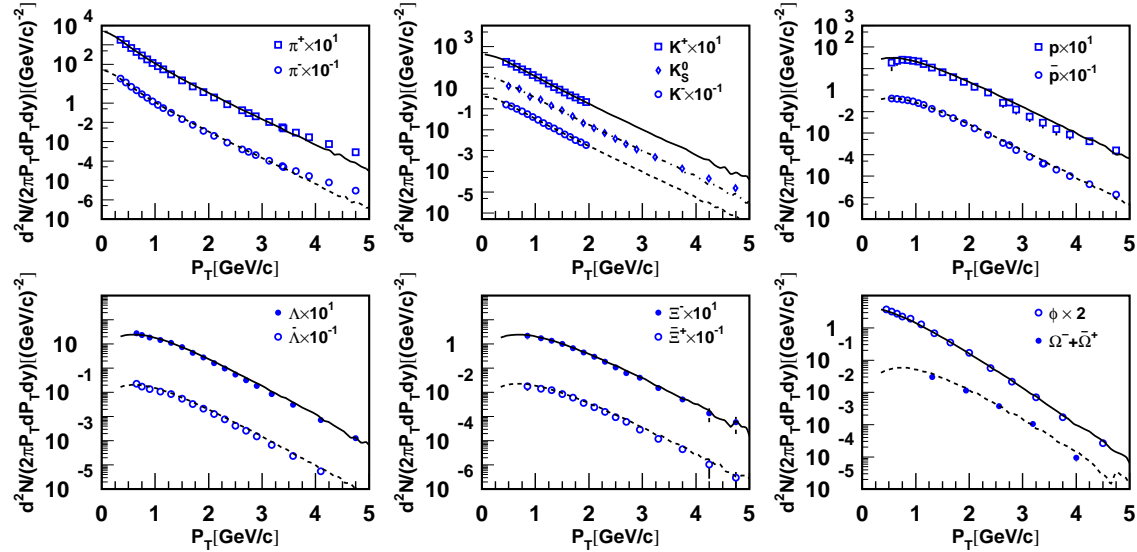


FIG. 5: (Color online) The transverse momentum distributions of identified hadrons at midrapidity in most central Au+Au collisions at  $\sqrt{s_{NN}} = 200$  GeV. Only the combination of thermal quarks is taken into account. Solid lines are the calculated results of hadrons and dashed lines for antihadrons. The experimental data are from Ref. [5, 53, 54]

increasing  $p_T$ . One can see that the experimental data in this region are well reproduced. The falling tendency of measured baryon/meson ratios after peak position is owing to the abundant participation of jet quarks, which is beyond the concern of the present paper. Besides the hadronization mechanism, the baryon/meson ratio in the intermediate  $p_T$  region is also influenced by other two factors. One is the nuclear stopping power in collisions. Comparing with the

strong collision transparency at top RHIC energy [39], the strong nuclear stopping at top SPS energy causes the detention of abundant net-quarks in the midrapidity region. These net-quarks significantly suppress the production of anti-baryons and enhance that of the baryons. Therefore, the  $\bar{p}/\pi^-$  ratio at top SPS energy is much lower than that at top RHIC energy while the  $\Lambda/K_s^0$  ratio at top SPS energy is higher than that at top RHIC energy. The other is the

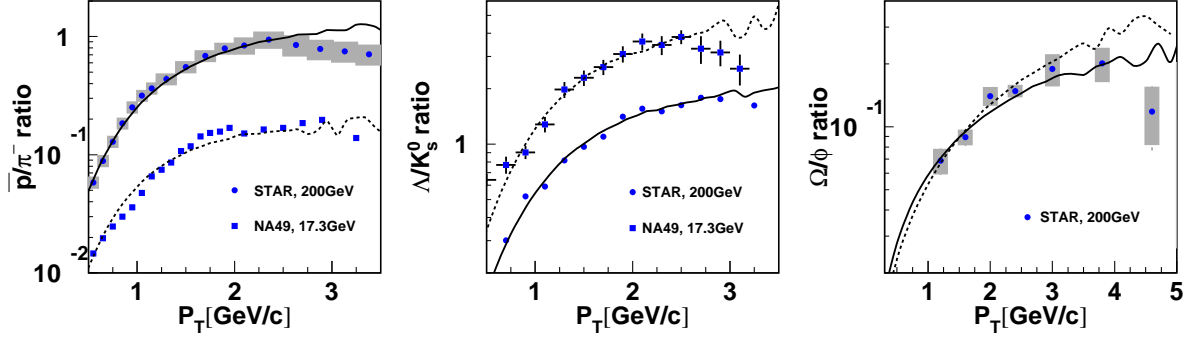


FIG. 6: (Color online) The ratios of  $\bar{p}/\pi^-$ ,  $\Lambda/K_s^0$  and  $\Omega/\phi$  at midrapidity in most central Pb+Pb collisions at  $\sqrt{s_{NN}} = 17.3$  GeV and Au+Au collisions at 200 GeV. Only the combination of thermal quarks is taken into account. Solid lines are the calculated results in Au+Au collisions and dashed lines for Pb+Pb collisions. The experimental data are from Ref. [5, 48, 54, 56, 57]

momentum distribution of constituent quarks at hadronization. This can be illustrated by  $\Omega/\phi$  ratio because the production of these two hadron species is less influenced by the net-quarks. The calculated  $\Omega/\phi$  ratio shows a weak dependence on the collision energy in the intermediate  $p_T$  range. The well description of various baryon/meson ratios in such a wide energy range is an indication of the universality for the quark combination mechanism.

## V. ANALYSIS OF PARTON DISTRIBUTIONS AT HADRONIZATION

The constituent quark distributions at hadronization carry the information on the evolution of the hot and dense quark matter in partonic phase. In this section, we focus attentions on the longitudinal and transverse collective flows and strangeness enhancement of the hot and dense quark matter produced at top SPS energy.

### A. The longitudinal and transverse collective flow

Due to the thermal pressure, the hot and dense quark matter created in high energy heavy ion collisions will expand during the evolution before hadronization. The longitudinal and transverse collective flow of final hadrons measured experimentally is the exhibition of this early thermal expansion in the partonic phase. Utilizing the relativistic hydrodynamic evolution of the hot and dense quark matter, one can obtain the collective flow in quark level from the extracted quark momentum distributions, and compare it with that at RHIC energies.

There are two well known hydrodynamic models for the description of the space time evolution of the hot and dense quark matter produced in heavy ion collisions. One is Bjorken model [58] which supposes that the collision is transparent, and it is appropriate to extremely high energy collisions, such as LHC. The other is Landau model [43] with an assumption of the full stopping for nucleus-

nucleus collisions. The longitudinal evolution result is equivalent to the superposition of a set of thermal sources in rapidity axis, with a (Bjorken) uniform or (Landau) Gaussian weight. In general, when applying the model to describe the hadron rapidity distributions, different parameter values are required to make a good fit of different hadron species [44]. In this paper, we apply the hydrodynamic description to the evolution in quark level, thus the collective flow of various hadrons can be coherently explained.

One can see from the energy dependence of the net-baryon rapidity distribution [39] that the collisions at top SPS energy are neither full transparent nor full stopping. The suppositions of nuclear stopping power in the two models are inappropriate to the nucleus-nucleus collisions at top SPS energy. For the description of the rapidity distribution for constituent quarks, one can limit the boost invariance into a finite rapidity range in the framework of Bjorken model. This modification is often used to analyze the longitudinal collectivity in hadronic level [44, 59]. The rapidity distribution in a isotropic, thermalized fluid element moving with a rapidity  $\eta$  is

$$\frac{dN_{th}}{dy}(y-\eta) = A T_f^3 \exp\left(-\frac{m}{T_f} \cosh(y-\eta)\right) \times \left(\frac{m^2}{T_f^2} + \frac{m}{T_f} \frac{2}{\cosh(y-\eta)} + \frac{2}{\cosh^2(y-\eta)}\right). \quad (7)$$

The rapidity distribution of constituent quarks in the hot and dense quark matter is the longitudinal boost-invariant superposition of multiple isotropic, thermalized fluid elements

$$\frac{dN}{dy} = \int_{-\eta_{max}}^{\eta_{max}} \frac{dN_{th}}{dy}(y-\eta) d\eta, \quad (8)$$

$\eta_{max}$  is the maximal boost rapidity of fluid elements. The average longitudinal collective velocity is taken to be  $<\beta_L> = \tanh(\eta_{max}/2)$ .

Here,  $T_f$  is the temperature of the locally-thermalized hot and dense quark matter at hadronization. It is taken to be  $T_f = 170$  MeV.  $m$  is the constituent mass of quarks

when they evolve to the transition point. It is taken to be 340 MeV for light quarks and 500 MeV for strange quarks. We have mentioned in above section that the net-quarks, still carrying a fraction of initial collision energy, have a more complex evolution than hydrodynamic expansion in longitudinal axis [60]. Therefore, we extract the longitudinal collective flow from the rapidity distribution of newborn quarks. Since most of the data are measured in the rapidity range about  $[-1.5, 1.5]$ , the rapidity spectra of constituent quarks extracted from experimental data are valid only in this region. Using above equations to fit the rapidity distribution of newborn constituent quarks in Fig. 1, we obtain  $\langle \beta_L \rangle = 0.58$  for light quarks and  $\langle \beta_L \rangle = 0.65$  for strange quarks. It is interesting to find that the average longitudinal collective velocity of strange quarks is obviously greater than that of light quarks.

For the transverse expansion of the hot and dense quark matter, we adopt a blast-wave model proposed by Heniz [59] within the boost-invariant scenario. The quarks and antiquarks transversely boost with a flow velocity  $\beta_r(r)$  as a function of transverse radial position  $r$ .  $\beta_r(r)$  is parameterized by the surface velocity  $\beta_s$ :  $\beta_r(r) = \beta_s \xi^n$ , where  $\xi = r/R_{max}$ , and  $R_{max}$  is the thermal source maximum radius ( $0 < \xi < 1$ ). The transverse momentum distribution of constituent quarks in the hot and dense quark matter can be equivalently described by a superposition of a set of thermalized fluid elements, each boosted with transverse rapidity  $\rho = \tanh^{-1}\beta_r$ ,

$$\frac{dN}{2\pi p_T dp_T} = A \int_0^1 \xi d\xi m_T \times I_0\left(\frac{p_T \sinh \rho}{T_f}\right) K_1\left(\frac{m_T \cosh \rho}{T_f}\right). \quad (9)$$

Here,  $I_0$  and  $K_1$  are the modified Bessel functions.  $m_T = \sqrt{p_T^2 + m^2}$  is the transverse mass of the constituent quark. The average transverse velocity can be written as

$$\langle \beta_r \rangle = \frac{\int \beta_s \xi^n \xi d\xi}{\int \xi d\xi} = \frac{2}{n+2} \beta_s. \quad (10)$$

With fixed parameter  $n = 0.3$ , the average transverse velocity  $\langle \beta_r \rangle$  is able to characterize the transverse collective flow of the hot and dense quark matter. Using the above equations to fit the transverse momentum distributions of the newborn quarks in Fig. 3, we obtain  $\langle \beta_r \rangle = 0.41$  for strange quarks and  $\langle \beta_r \rangle = 0.36$  for light quarks. One can see that the  $\langle \beta_r \rangle$  of strange quarks is obviously greater than that of light quarks.

Both longitudinal and transverse results at top SPS energy show that the strange constituent quarks get a stronger collective flow than the light quarks in the hydrodynamic evolution of partonic matter. By analyzing the data of multi-strange hadrons [26] and primary charged hadrons [23], the same property is found also at top RHIC energy. It suggests that the hot and dense quark matter produced at top SPS energy undergoes a similar hydrodynamic evolution to that at RHIC energies. It is generally believed that the decoupled quark and gluon plasma (QGP) has been created at RHIC energies [61]. This similarity of collective

flow property in quark level may be regarded as a signal of QGP creation at top SPS energy.

## B. The enhanced strangeness

An interesting phenomenon in high energy heavy ion collisions is the enhanced production of strange hadrons, which is absent in elementary particle collisions. In relativistic heavy ion collisions, enormous amounts of energy are deposited in the collision region to create a deconfined hot and dense quark matter. The multiple scatterings between partons in the hot and dense quark matter will cause the large production rate of strangeness by  $gg \rightarrow s\bar{s}$  [27]. The high strangeness of the hot and dense quark matter, after hadronization, finally leads to the abundant production of the strange hadrons. This phenomenon is regarded as a signal of QGP creation. As we know, the enhancement of strangeness production at top RHIC energy is quite obvious [62], and it is generally believed that the QGP has been created at RHIC energies. When the collision energy drops to the SPS and AGS energies, it is found that the strangeness production peaks at about 30A GeV and turns into a plateau at higher collision energies [14]. It is an indication of the onset of deconfinement.

In our model, the strangeness of the hot and dense quark matter is characterized by the suppression factor  $\lambda_s = N_{\bar{s}} : N_{\bar{u}} = N_{\bar{s}} : N_{\bar{d}}$ , i.e. the ratio of  $s$  quark number to newborn  $u$  (or  $d$ ) quark number. By fitting the experimental data of identified hadrons, we use the model to extract the  $\lambda_s$  of hot and dense quark matter at midrapidity in central AA collisions at four energies  $\sqrt{s_{NN}} = 17.3, 62.4, 130$  and  $200$  GeV, and the results are shown in Table III. The data of midrapidity  $dN/dy$  and the calculated results with minimum deviations at different collision energies are shown also. The statistical uncertainty of  $\lambda_s$  is fixed by the twice minimum deviation. The model reproduces the hadron yield in reasonably good way, and the chi-square fit seems to indicate that with increasing collision energy the agreement with data significantly improves.

One can see that  $\lambda_s$  in such a broad energy range is nearly unchanged within statistical uncertainties, exhibiting an obvious saturation phenomenon. The results of  $\lambda_s$  are consistent with the grand canonical limit ( $\approx 0.45$ ) of strangeness [15]. Using the Bjorken model, one can estimate that the primordial spatial energy density of the hot and dense quark matter produced in collisions at top RHIC energy is about  $6.0 \text{ GeV}/fm^3$  [15], double of that in Pb+Pb collisions at top SPS energy. The difference in primordial energy density is large while the final strangeness is nearly equal. The hot and dense quark matter created in heavy ion collisions is shown to be very close to a perfect fluid [71]. It means that the local relaxation time toward to thermal equilibrium is much shorter than the macroscopic evolution time of the hot and dense quark matter. When the hot and dense quark matter evolves to the point of hadronization, the strangeness abundance should be mainly determined by the current temperature, irrelevant to the initial



TABLE III: The strange suppression factor  $\lambda_s$  and the calculated hadron  $dN/dy$  at midrapidity in central AA collisions at different energies. The experimental data are taken from Ref. [32, 36, 37, 53, 63, 64, 65, 66, 67, 68, 69, 70].

Pb Pb 17.3 GeV			Au Au 62.4 GeV		Au Au 130 GeV		Au Au 200 GeV	
	data	model	data	model	data	model	data	model
$\pi^+$	$170.1 \pm 0.7 \pm 9$	168.3	$212 \pm 5.8 \pm 14$	211	$276 \pm 3 \pm 35.9$	268.7	$286.4 \pm 24.2$	287.3
$\pi^-$	$175.4 \pm 0.7 \pm 9$	183.5	$204 \pm 7.4 \pm 14$	217	$270 \pm 3.5 \pm 35.1$	272.4	$281.8 \pm 22.8$	288.3
$K^+$	$29.6 \pm 0.3 \pm 1.5$	27.3	$33.35 \pm 2.15$	36.3	$46.7 \pm 1.5 \pm 7$	46.6	$48.9 \pm 6.3$	48.35
$K^-$	$16.8 \pm 0.2 \pm 0.8$	15.7	$28.16 \pm 1.76$	29.9	$40.5 \pm 2.3 \pm 6$	43.1	$45.7 \pm 5.2$	46.48
$p$	$29.6 \pm 0.9 \pm 2.9$	25.9	$27 \pm 1.8 \pm 4.6$	26.17	$19.3 \pm 0.6 \pm 3.3$	16.45	$18.4 \pm 2.6$	17.41
$\bar{p}$	$1.66 \pm 0.17 \pm 0.16$	1.53	$11.5 \pm 1.5 \pm 2.9$	11.15	$13.7 \pm 0.7 \pm 2.3$	11.63	$13.5 \pm 1.8$	13.48
$\Lambda$	$9.5 \pm 0.1 \pm 1$	13.3	$14.9 \pm 0.2 \pm 1.49$	13.42	$17.3 \pm 1.8 \pm 2.7$	14.99	$16.7 \pm 0.2 \pm 1.1$	15.76
$\bar{\Lambda}$	$1.24 \pm 0.03 \pm 0.13$	1.35	$8.02 \pm 0.11 \pm 0.8$	6.77	$12.7 \pm 1.8 \pm 2$	11.4	$12.7 \pm 0.2 \pm 0.9$	12.6
$\Xi^-$	$1.44 \pm 0.1 \pm 0.15$	1.43	$1.64 \pm 0.03 \pm 0.014$	1.63	$2.04 \pm 0.14 \pm 0.2$	1.99	$2.17 \pm 0.06 \pm 0.19$	2.12
$\Xi^+$	$0.31 \pm 0.03 \pm 0.03$	0.26	$0.989 \pm 0.057 \pm 0.057$	0.96	$1.74 \pm 0.12 \pm 0.17$	1.67	$1.83 \pm 0.05 \pm 0.2$	1.72
$\Omega + \bar{\Omega}$		0.17	$0.356 \pm 0.046 \pm 0.014$	0.369	$0.56 \pm 0.11 \pm 0.05$	0.551	$0.53 \pm 0.04 \pm 0.04$	0.539
$\chi^2/ndf$	10.7/7		6.2/8		1.6/8		0.88/8	
$\lambda_s$	$0.48 \pm 0.09$		$0.44 \pm 0.02$		$0.44 \pm 0.04$		$0.42 \pm 0.025$	

energy density and temperature. The same strangeness is an indication of the universal hadronization temperature for the hot and dense quark matter with low baryon chemical potential.

## VI. SUMMARY

In this paper, we have systematically studied the longitudinal and transverse production of various hadrons at top SPS energy in the scheme of quark combination. Using the quark combination model, we firstly calculate the yields and rapidity distributions of various hadrons in most central Pb+Pb collisions at  $\sqrt{s_{NN}} = 17.3$  GeV. The calculated results are in agreement with the experimental data. This indicates that the quark combination mechanism is applicable in describing the longitudinal hadron production at this collision energy. Secondly the  $p_T$  distributions of various hadrons at top SPS energy are calculated and compared with the data. It is found that the light, single and multi-strange hadrons are well reproduced by the same quark distributions. It indicates that the hadronization of the hot and dense quark matter is a rapid process. The well reproduced baryon/meson ratios in the interme-

diate  $p_T$  range at different collision energies are indicative of the universality for the quark combination mechanism. By fitting the extracted constituent quark distributions at hadronization with the hydrodynamic scenario, we further obtain the longitudinal and transverse collective flow of the hot and dense quark matter produced at top SPS energy. It is found that the strange quarks get a stronger collective flow than light quarks, which is consistent with that at RHIC energies. The strangeness in the hot and dense quark matter produced at  $\sqrt{s_{NN}} = 17.3, 62.4, 130, 200$  GeV are extracted. The almost unchanged strangeness may be associated with a universal hadronization temperature for the hot and dense quark matter with low baryon chemical potential.

## ACKNOWLEDGMENTS

The authors thank Q. Wang, Z. T. Liang and R. Q. Wang for helpful discussions. The work is supported in part by the National Natural Science Foundation of China under the grant 10775089 and the science fund of Qufu Normal University.

- 
- [1] L. Susskind, Phys. Rev. D **20** 2610 (1979).
  - [2] F. Karsch and E. Laerman, in *Quark-Gluon Plasma 3*, edited by R.C. Hwa and X. N. Wang ( World Scientific 2004), p.1.
  - [3] M. Gyulassy and L. McLerran, Nucl. Phys. A **750**, 30 (2005).
  - [4] X. N. Wang, Phys. Rev. C **58**, 2321 (1998).
  - [5] B. I. Abelev, *et al.* (STAR Collaboration), Phys. Rev. Lett. **97**, 152301 (2006).
  - [6] A. Adare, *et al.* (PHENIX Collaboration), Phys. Rev. Lett. **98**, 162301 (2007).
  - [7] R. J. Fries, B. Müller, C. Nonaka, and S. A. Bass, Phys. Rev. Lett. **90**, 202303 (2003).
  - [8] V. Greco, C. M. Ko, and P. Lévai, Phys. Rev. Lett. **90**, 202302 (2003).
  - [9] R. J. Fries, B. Müller, C. Nonaka, and S. A. Bass, Phys. Rev. C **68**, 044902 (2003).
  - [10] V. Greco, C. M. Ko, and P. Lévai, Phys. Rev. C **68**, 034904 (2003).
  - [11] Rudolph C. Hwa and C. B. Yang, Phys. Rev. C **70**, 024905 (2004).

- [12] Rudolph C. Hwa and Li-Lin Zhu, Phys. Rev. C **78**, 024907 (2008).
- [13] C. Alt *et al.* (NA49 Collaboration), Phys. Rev. C **75**, 044901 (2007).
- [14] C. Alt *et al.* (NA49 Collaboration), Phys. Rev. C **77**, 024903 (2008).
- [15] Reinhard Stock, arXiv: nucl-ex/0807.1610v1 (2008).
- [16] D. Molnar and S. A. Voloshin, Phys. Rev. Lett. **91**, 092301 (2003).
- [17] C. B. Yang, J. Phys. G **32** L11 (2006).
- [18] Q. B. Xie and X. M. Liu, Phys. Rev. D **38**, 2169 (1988).
- [19] F. L. Shao, Q. B. Xie and Q. Wang, Phys. Rev. C **71**, 044903 (2005).
- [20] F. L. Shao, T. Yao, and Q. B. Xie, Phys. Rev. C **75**, 034904 (2007).
- [21] T. Yao, Q. B. Xie and F. L. Shao, Chinese Physics C **32**, 356 (2008).
- [22] T. Yao, W. Zhou and Q. B. Xie, Phys. Rev. C **78**, 064911 (2008); E. S. Chen, Sci. China, **33**, 955 (1990).
- [23] Y. F. Wang *et al.*, Chinese Physics C **32** 976 (2008).
- [24] T. S. Biró, Lévai and J. Zimányi, Phys. Lett. B **347** 6 (1995).
- [25] J. Zimányi, T. S. Biró, T. Csörgő and Lévai and, Phys. Lett. B **472** 243 (2000).
- [26] J. H. Chen *et al.*, Phys. Rev. C **78**, 034907 (2008).
- [27] J. Rafelski and B. Müller, Phys. Rev. Lett. **48** 1066 (1982).
- [28] Q. B. Xie, Proceedings of the 19th International Symposium on Multiparticle Dynamics, Arles, France, 1988, edited by D. Schiff and J. Tran Thanh Vann (world scitific, 1988) p369.
- [29] Q. Wang and Q. B. Xie, J. Phys. G **21**, 897 (1995).
- [30] Review of Particle Physics, Particle Data Group, Phys. Lett. B **667** 1 (2008).
- [31] W. Hofmann, Ann. Rev. Nucl. Part. Sci. **38**, 279 (1988).
- [32] S. V. Afanasiev *et al.* (NA49 Collaboration), Phys. Rev. C **66**, 054902 (2002).
- [33] H. Appelshäuser *et al.* (NA49 Collaboration), Phys. Rev. Lett. **82**, 2471 (1999).
- [34] F. Antinori *et al.* (NA57 Collaboration), J. Phys. G **31** 1345 (2005).
- [35] C. Alt *et al.* (NA49 Collaboration), Phys. Rev. C **78**, 044907 (2008).
- [36] C. Alt *et al.* (NA49 Collaboration), Phys. Rev. C **73**, 044910 (2006).
- [37] C. Alt *et al.* (NA49 Collaboration), Phys. Rev. C **78**, 034918 (2008).
- [38] A. Mischke for the NA49 Collaboration, Nucl. Phys. A **715** 453c (2003).
- [39] I. G. Bearden *et al.* (BRAHMS Collaboration), Phys. Rev. Lett. **93**, 102301 (2004).
- [40] M. Hirai, S. Kumano, M. Oka, and K. Sudoh, Phys. Rev. D **77**, 017504 (2008).
- [41] P. Fachini for the STAR Collaboration, Nucl. Phys. A **715** 462c (2003).
- [42] J. Adams *et al.* (STAR Collaboration), Phys. Lett. B **612** 181 (2005).
- [43] L. D. Landau, Izv. Akad. Nauk Ser. Fiz. **17**, 51 (1953); in Collected Papers of L. D. Landau (Pergamon, Oxford, 1965), p. 665.
- [44] B. Mohanty and Jan-e Alam, Phys. Rev. C **68**, 064903 (2003).
- [45] L. M. Satarov, I. N. Mishustin, A. V. Merdeev, and H. Stöcker, Phys. Rev. C **75**, 024903 (2007).
- [46] E. K. G. Sarkisyan and A. S. Sakharov, AIP Conf. Proceedings **828**, 35-41 (2006); hep-ph/0410324, CERN-PH-TH/2004-213.
- [47] S. V. Afanasiev *et al.* (NA49 Collaboration), Phys. Lett. B **491** 59 (2000).
- [48] C. Alt *et al.* (NA49 Collaboration), Phys. Rev. C **77**, 034906 (2008).
- [49] T. Anticic *et al.* (NA49 Collaboration), Phys. Rev. Lett. **93** 022302 (2004).
- [50] C. Alt *et al.* (NA49 Collaboration), Phys. Rev. Lett. **94** 192301 (2005).
- [51] B. Alessandro *et al.* (NA50 Collaboration), Phys. Lett. B **555** 147 (2003).
- [52] H. van Hecke, H. Sorge, and N. Xu, Phys. Rev. Lett. **81** 5764 (1998).
- [53] J. Adams, *et al.* (STAR Collaboration), Phys. Rev. Lett. **98**, 062301 (2007).
- [54] B. I. Abelev, *et al.* (STAR Collaboration), Phys. Rev. Lett. **99**, 112301 (2007).
- [55] J. Song, F. L. Shao and X. B. Xie, Int. J. Mod. Phys. A **24** 1161 (2009).
- [56] B. I. Abelev, *et al.* (STAR Collaboration), arXiv: nucl-ex/0601042 (2006).
- [57] András László and Tim Schuster for the NA49 Collaboration, Nucl. Phys. A **774** 473 (2006).
- [58] J. D. Bjorken, Phys. Rev. D **27** 140 (1984).
- [59] E. Schnedermann, J. Sollfrank, and U. Heinz, Phys. Rev. C **48**, 2462 (1993).
- [60] G. Wolschin, Phys. Rev. C **69**, 024906 (2004).
- [61] M. Gyulassy and L. McLerran, Nucl. Phys. A **750** 30 (2005).
- [62] B. I. Abelev *et al.* (STAR Collaboration), Phys. Rev. C **77** 044908 (2008).
- [63] I. C. Arsene (for BRAHMS Collaboration) J. Phys. G **35** 104056 (2008).
- [64] B. I. Abelev *et al.* (STAR Collaboration), Phys. Lett. B **655** 104 (2007).
- [65] J. Takahashi (for the STAR Collaboration), J. Phys. G **31** s1061 (2005).
- [66] Jeff Speltz (for the STAR Collaboration), J. Phys. G **31** s1025 (2005).
- [67] K. Adcox *et al.* (PHENIX Collaboration), Phys. Rev. C **69** 024904 (2004).
- [68] K. Adcox *et al.* (PHENIX Collaboration), Phys. Rev. Lett. **89** 092302 (2002).
- [69] J. Adams *et al.* (STAR Collaboration), Phys. Rev. Lett. **92** 182301 (2004).
- [70] S. S. Adler *et al.* (PHENIX Collaboration), Phys. Rev. C **69** 034909 (2004).
- [71] Huichao Song, and U. Heinz, Phys. Rev. C **77** 064901 (2008).